COMMUNICATION

Check for updates

Stereospecific synthesis of chiral P-containing polyaromatics based on 7-membered P-rings†

Réka Mokrai, [abc] Anabella Mocanu,[a] Matthew P. Duffy,[a] Thomas Vives,[a] Elsa Caytan,[a] Vincent Dorcet,[a] Thierry Roisnel,[a] László Nyulászi,[bc] Zoltán Benkő, *[b] Pierre-Antoine Bouit *[a] and Muriel Hissler *[a]

We present the stereospecific synthesis of helicenoid-based phosphepines (7-membered P-rings) as well as chiral P-containing polycyclic aromatic hydrocarbons. In these systems, an axial to central chirality transfer takes place from the BINAP moiety to the P-atom. The impact of the molecular design on the structure, the (chir)optical (including circularly polarized luminescence) and redox properties are investigated.

Polycyclic aromatic hydrocarbons (PAHs) with fused-benzene rings have been widely investigated due to their potential applications in optoelectronic devices.[1] The properties of PAHs are determined by their molecular structure which is mainly defined by their fusion pattern: *ortho-* and peri-fused systems possess a polyaromatic framework which can be planar (PAH **A**)[1] or helicoidal (PAH **B**) (Fig. 1).[2] The insertion of non-benzenoids rings in the framework is another way to tune the properties since a deviation of the planarity (for example **C**, Fig. 1) modifies the π-systems leading to potentially chiral compounds.[3] In most of the cases, stereospecific access to such compounds is difficult. In the meantime, chiral π-conjugated systems appeared as promising building blocks in organic electronics, nanotechnology, sensing or catalysis.[4] Another approach to tune the properties of π-systems is to introduce heterocycles within the C-framework.[5] Recently, the phosphepine ring (7-membered unsaturated P-ring, **D**, Fig. 1) also gained attention for its potential applications in optoelectronics.[6] Its distorted framework allows the preparation of twisted π-systems that were successfully introduced into OLEDs

or OFETs. The 7-membered P-ring is a potential source of chirality that has not been exploited so far in the field of molecular materials.[7] In the present article, we describe the stereospecific synthesis of helicenoid-based phosphepine as well as a chiral P-containing PAH through an axial to central chirality transfer from readily available 2,2′-bis(diphenyl-phosphino)-1,1′-binaphthalene (BINAP). The impact of the molecular design on the structure, the (chir)optical and redox properties are investigated using a joint experimental/theoretical approach, highlighting the potential of these chiral derivatives for further applications in optoelectronics or catalysis.

For the synthesis, we adapted Widhalm's strategy, developed originally for a racemic phosphepine-based helicenoid structure ((R_P,M)-**1**/(S_P,P)-**1**, abbreviated rac-**1** for simplicity, Scheme 1).[8–11] Using enantiopure BINAP-oxides as starting materials, we observed that the reaction is fully stereospecific (see ESI† for chiral supercritical fluid chromatography (SFC)) and, thus, afford enantiopure compounds (R_p,M)-**1** in 54% yield and (S_p,P)-**1** in 63% yield. Enantiomers of **1** were fully

[a] *Univ Rennes, CNRS, ISCR–UMR 6226, Rennes F-35000, Hungary.*
  E-mail: muriel.hissler@univ-rennes1.fr

[b] *Department of Inorganic and Analytical Chemistry,*
  Budapest University of Technology and Economics, Szt. Gellért tér 4,
  Budapest H-1111, Hungary. E-mail: zbenko@mail.bme.hu

[c] *MTA-BME Computation Driven Chemistry Research Group. Szt. Gellért tér 4,*
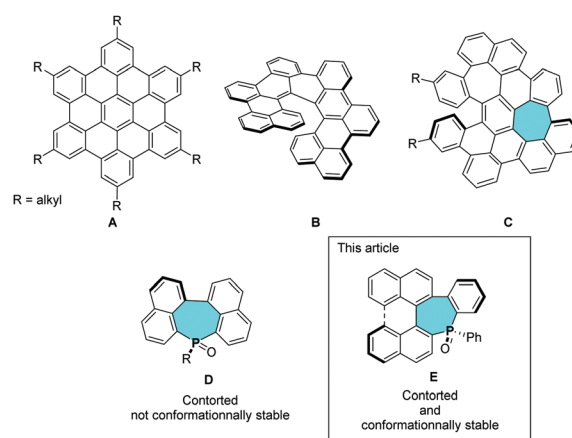 *Budapest H-1111, Hungary*

Fig. 1 Up: Example of fully benzenoid planar PAH (A) and chiral (B); chiral PAH featuring 7-membered ring (C). Down: PAH featuring 7-membered P-ring (D) and structures (E) studied in this article.
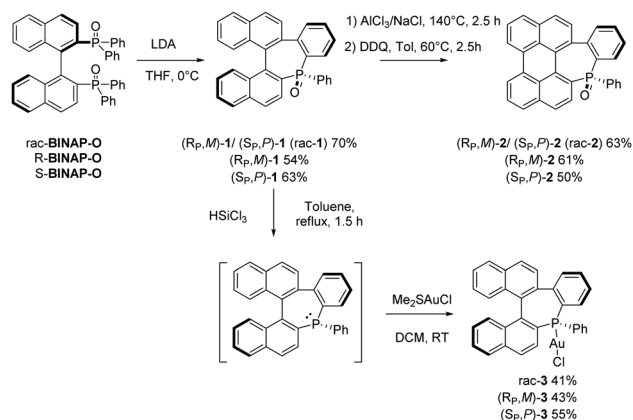
Scheme 1   Synthesis of **1–3**.

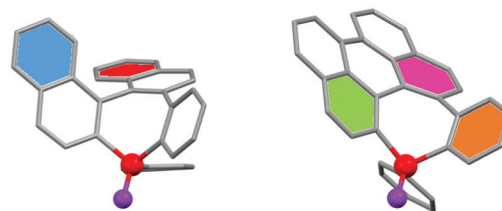Fig. 2   X-Ray crystallographic structure of (R_P, M)-**1** (left) and (R_P, M)-**2** (right).

characterized by multinuclear NMR spectroscopy and MS analysis and additionally by single-crystal X-ray diffraction. Based on X-ray analysis (*vide infra*), the use of (R)-BINAP leads to the formation of (R_P, M)-**1** in which the P center has a R configuration and the helicenoid backbone forms a left-handed helix and thus adopts a M configuration. The (S)-BINAP leads to the formation of (S_P, P)-**1** in 63% yield. In these systems, an axial to central chirality transfer takes place as the BINAP moiety controls the stereochemistry of the P-atom.[12]

The binaphthyl backbone of rac-**1** was further fused in "Scholl conditions" to afford the perylene fused phosphepine ((R_P,M)-**2**/(S_P,P)-**2**, abbreviated rac-**2**) in 63% yield (Scheme 1). The reaction carried out with the enantiopure starting materials affords (R_P,M)-**2** (61%) and (S_P,P)-**2** (50%) with retention of the configuration at the P and the helicenoid part (see X-ray). Again, the enantiopurity was checked by chiral SFC.

The conformational stability of these chiral compounds was confirmed as no sign of epimerization was observed upon heating the compounds at 140 °C (for 2.5 hours) during the synthesis. For both **1** and **2** scaffolds, we have calculated the activation barriers for the inversion of configuration of the PAH backbone and the resulting products at the B3LYP-D3/cc-pVDZ level. The inversion barrier for the helical backbone in the case of (S_P,P)-**1** (leading to (S_P,M)-**1**) is 46.2 kcal mol^{-1}, which is larger than the racemization barrier of [5]helicene (E_a = 23.5 kcal mol^{-1}) or [6]helicene (E_a = 35.0 kcal mol^{-1}) (Fig. S29–S31 and Table S4, ESI†).[13]

This confirms that insertion of heptagons allows obtaining conformationally stable [5]helicene without functionalization in the fjord position (unlike carbo[5]helicenes).[3c,14] The formation of the new C–C bond decreases the inversion barrier for (R_P,M)-**2** to 32.5 kcal mol^{-1}.

To illustrate the versatility of the synthetic approach and offer post-functionalization possibilities, phosphepine oxide rac-**1**, (R_P, M)-**1** and (S_P, P)-**1** were reduced to the corresponding σ^3, λ^3-analogues. These intermediates were directly complexed to Au^I to afford rac-**3**, (R_P, M)-**3** and (S_P, P)-**3** by reacting with Me$_2$SAuCl (Scheme 1). The enantiopurity and the retention of the configuration (both the helicenoid fragment and the P-atom) were confirmed by chiral SFC and X-ray analysis

(Fig. S9 and S10, ESI†). This confirms the conformational stability of the compounds even in their trivalent form and, thus paves the way toward the stereospecific synthesis of a great diversity of chiral coordination complexes.

The molecular structures of derivatives **1–3** were all confirmed by single-crystal X-ray diffraction (Fig. 2). The study will focus on **1** and **2** as the structure of complex **3** is similar to **1**. In all of these compounds, the σ^4,λ^5-P atom is in a tetrahedral coordination environment with usual valence angles and C–P bond lengths. As reported by Widhalm[7] rac-**1** crystallizes as a conglomerate and the analyzed crystal revealed the presence of only the (R_P, M)-enantiomer. The X-ray structures of (R_P, M)-**1** and (S_P, P)-**1** confirm the helicenoid arrangement of the rings with a "helicity" angle of respectively 68.2° and 68.1° (angle between the two rings at each extremity of the helix, represented here in blue and red, Fig. 2). The seven-membered rings present the expected boat-like conformation with the phenyl substituents on the P-atom in axial position. Intramolecular π-stacking between this exocyclic *P*-phenyl and one of the naphthyl fragments (*d* = 3.55 Å for (R_P, M)-**1** and *d* = 3.56 Å for (S_P, P)-**1**) takes place (Fig. S11, ESI†). The structure of rac-**2** consists of a racemic mixture of the two enantiomers. This derivative is a contorted PAH featuring a negative curvature with angles between the phenyl ring situated at the 2–3 (in green, Fig. 2) and 6–7 position (in orange, Fig. 2) of 111.2° and angle between the phenyl at the 4–5 position (in purple) and the mean phosphepine plane of 149.3° in the opposite direction. Again, the seven-membered ring displays a boat-like conformation with the *P*-phenyl substituents in axial position. In this case, no intramolecular π-stacking is observed. This structural part highlights the fact that molecular engineering of polyaromatic phosphepines allows preparing derivatives with a great structural variety such as helicenoid derivatives and negatively curved PAH.

The spectroscopic properties of all compounds were investigated in diluted CH$_2$Cl$_2$ solutions (*c* = 5 × 10^{-6} mol L^{-1}, Fig. 3 and Table S2, ESI†) at room temperature. rac-**1**, (S_P, P)-**1** and (R_P, M)-**1** display almost identical UV/Vis spectra consisting of a strong absorption band at 260 nm (ε = 3.6 × 10^4 M^{-1} cm^{-1}) and several bands of medium and low intensity (4 × 10^3 M^{-1} cm^{-1} < ε < 14 × 10^3 M^{-1} cm^{-1}) from 282 to 334 nm (Fig. 3). TD-DFT calculations employing different functionals (B3LYP, ωB97XD, M06-2X, cam-B3LYP) and ADC(2) calculations predict similar excitation energies as observed in the experimental spectrum. The best overall fit was found at the TD-B3LYP/6-31G* level,
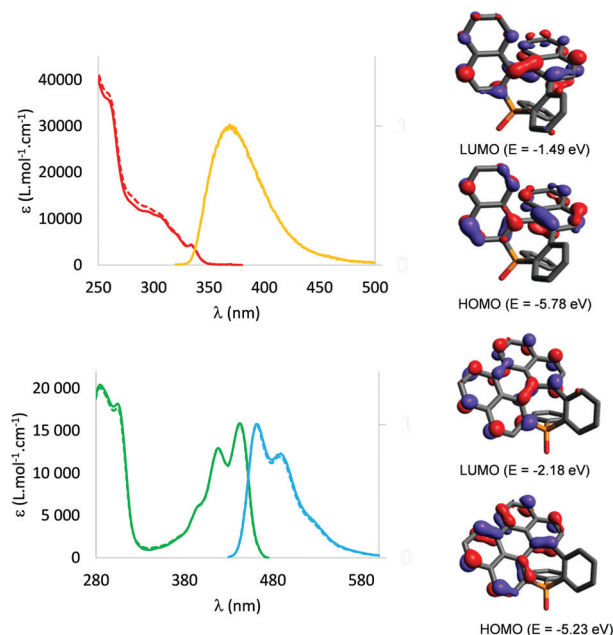
LUMO (E = -1.49 eV)

HOMO (E = -5.78 eV)

LUMO (E = -2.18 eV)

HOMO (E = -5.23 eV)

Fig. 3 UV-Vis absorption and normalized emission spectra of (S_P, P)-**1** (dotted) and (R_P, M)-**1** (solid line) in CH_2Cl_2 (c = 5 × 10^{-6} M). HOMO and LUMO of **1** (up) UV-Vis absorption and normalized emission spectra of (S_P, P)-**2** (dotted) and (R_P, M)-**2** (solid line) in CH_2Cl_2 (c = 5 × 10^{-6} M). HOMO and LUMO of **2** (down) (calculations at the B3LYP/6-31G*//B3LYP/6-31+G* level).

Fig. 4 ECD spectra of (R_P, M)-**1** (red), (S_P, P)-**1** (red, dotted) - (R_P,M)-**2**, (green) (S_P,P)-**2** (green, dotted) in diluted DCM at 10^{-5} M.

which shows two strong absorption bands at 263 and 256 nm (oscillator strength: f = 0.137 and f = 0.111, respectively) as well as four closely spaced transitions with lower oscillator strength in the 331 and 272 nm region (for details see ESI†). At this level of theory, the S_1 state (at 331 nm) corresponds to a HOMO–LUMO transition (Fig. 3) involving the π system with a modest oscillator strength (f = 0.086). The absorption bands are associated with several, near lying π–π* electronic transitions of the helicenoid backbone without contribution of the P-atom indicating that these properties are predominantly determined by the helical π-electron system of such compounds, in accordance to the non aromatic NICS values of the seven membered ring as shown in Fig. S33 of the ESI.†

The emission properties of rac-**1**, (S_P, P)-**1** and (R_P, M)-**1** were, then, examined in CH_2Cl_2 at a concentration of 10^{-5} M. At RT, all compounds behave as blue fluorescent emitters, with emission wavelengths at 371 nm and a quantum yield of 18% in solution. The insertion of a phosphepine in the helicenoid structure induced a blue-shift of the emission maximum and increased emission performance compared to [5]helicene (λ_{em} = 424 nm, ϕ = 4%).[15] All compounds also luminesce as powders (Fig. S18, ESI†). To get more insights into the impact of chirality on the properties of these systems, electronic circular dichroism (ECD) spectra have been recorded in diluted DCM solutions. Firstly, (R_P, M)-**1** and (S_P, P)-**1** displayed ECD with the expected mirror-image relationship (Fig. 4). For example, (R_P, M)-**1** displays a strong negative ECD band ($\Delta\varepsilon$ = −99.0 at 252 nm) and a positive band ($\Delta\varepsilon$ = 6.4 M^{-1} cm^{-1} at 330 nm). The spectra were nicely fitted by DFT calculations. In both
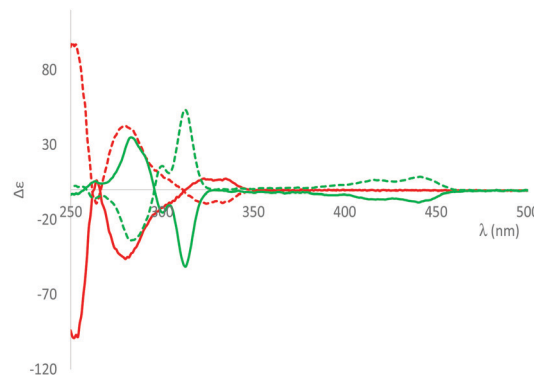
cases, the lowest energy ECD bands are attributed to HOMO–LUMO transitions. (R_P, M)-**1** (resp. (S_P, P))-**1** display also CPL with g_{lum} ∼ 2 × 10^{-3} at 385 nm (Fig. S27, ESI†). These values are rather classical for organic CPL emitters[16] but higher than previously reported organophosphorus based-organic CPL emitter.[17] This first result thus paves the way toward the introduction of optimized helical phosphepine into chiroptical devices.

Rac-**2**, (S_P, P)-**2** and (R_P, M)-**2**, having a smaller "helicity" angle (*vide supra*) and thus a larger π-conjugated platform than their helicenoid precursor, exhibit markedly different optical and redox properties. The UV-vis absorption spectra of (R_P,M)-**2**, (S_P,P)-**2** and *rac*-**2** display a structured absorption band in the visible (λ_{max} = 441 nm, Fig. 3), characteristic of their perylene-based structure (Fig. S17, ESI†). The TD-DFT calculations show that this absorption is attributed to an intense π–π* HOMO–LUMO transition at 442 nm (f = 0.238) of the perylene backbone without any significant contribution of the P-atom (Table S8, ESI†). The red-shift is easily rationalized by the extension of the conjugation between compounds **1** and **2**. Compounds **2** display strong luminescence in solution with the same gradual red-shift (λ_{em} (rac-**1**) = 371 nm and λ_{em} (rac-**2**, (R_P,M)-**2**, (S_P,P)-**2**) = 461 nm). It is noteworthy that **2** displays excellent fluorescence quantum yield in solution (ϕ = 79%). Interestingly, despite its polyaromatic platform, **2** also luminesce in the solid-state without noticeable impact of the chirality (Fig. S19, ESI†). (R_P,M)-**2** displays a strong negative structured ECD band ($\Delta\varepsilon$ = −50.4 M^{-1} cm^{-1} at 313 nm) followed by another negative structured band in the visible ($\Delta\varepsilon$ = −8.31 M^{-1} cm^{-1} at 440 nm) (Fig. 4). The spectra were nicely fitted by DFT calculations. Again, the lowest energy ECD bands are attributed to HOMO–LUMO transitions. This red-shift compared to **1** is again attributed to a larger π-platform. In addition, the CPL of R_P,M-**2** (resp. S_P,P-**2**) was too weak to be accurately measured (g_{lum} < 10^{-4}). The weaker chiroptical properties of **2** (g_{abs} = 5 × 10^{-4} at 442 nm; g_{lum} < 10^{-4}) compared to helicenoids **1** (g_{abs} = 2 × 10^{-3} at 330 nm; g_{lum} = 2 × 10^{-3} at 385 nm) are in accordance with the fact that these π–π* transitions are localized mainly on the nearly planar perylene backbone (Fig. 3) and are rather far from the source of chirality.

However, these data nicely illustrate that the presence of the 7-membered P-ring endows the perylene scaffold with appealing chiroptical properties.

The electrochemical behaviour of rac-**2** was investigated by cyclic voltammetry in DCM. While rac-**1** does not display any redox processes in these experimental conditions, rac-**2** displays quasi-reversible oxidation (E_{ox} = +0.84 V $vs.$ Fc$^+$/Fc) and reduction (E_{red} = −1.94 V $vs.$ Fc$^+$/Fc) (Fig. S12, ESI†). In particular, reduction is easier (ΔE_{red} = 0.3 V) than for perylene due to the electron-withdrawing P=O moiety (Fig. S13, ESI†). The HOMO and the LUMO are of π-type orbitals located on the contorted perylene fragment of rac-**2**. By the formation of the fused C–C bond the HOMO–LUMO gap significantly decreases compared to rac-**1** due to the destabilization of the HOMO and stabilization of the LUMO levels upon formation of the non-aromatic middle ring (Fig. S28, ESI†). Spectroelectrochemical measurements reveal that oxidation/reduction is accompanied by the apparition of new transitions at ∼600 nm (Fig. S21 and S22, ESI†), as expected for π-conjugated radicals. DFT calculations confirm that in the radical ions the spin density is delocalized on the π-platform (Fig. S34, ESI†). However, such new transition is not CD-active (Fig. S26, ESI†). In conclusion, the study of the properties on rac-**2**, (S_P, P)-**2** and (R_P, M)-**2** illustrates that these polyaromatic phosphepines display perylene-like properties (strong absorption/emission) as well as reversible redox and chiroptical properties directly arising from the presence of the 7-membered P-ring.

In the present article, we describe the stereospecific synthesis of helicenoid-based phosphepine **1**, as well as coordination complexes **3**, and chiral P-containing PAH **2**. In these systems, an axial to central chirality transfer takes place from the BINAP moiety to the P-atom. The impact of the molecular design on the structure, the (chir)optical and redox properties are investigated. The modification of the aromatic platform allows tuning the properties with helicenoid **1** having favorable chiroptical properties including CPL emission. Due to its large π-platform associated with an electro-withdrawing P=O group, **2** displays high luminescence and reversible electrochemical properties. These structure–property relationships highlight the great potential of these chiral derivatives for further applications in optoelectronics or (organometallic) catalysis.

Conflicts of interest

There are no conflicts to declare.

Notes and references

1 J. Wu, W. Pisula and K. Müllen, *Chem. Rev.*, 2007, **107**, 718.
2 (a) Y. Nakakuki, T. Hirose, H. Sotome, H. Miyasaka and K. Matsuda, *J. Am. Chem. Soc.*, 2018, **140**(12), 4317–4326; (b) Y. Zhu, Z. Xia, Z. Cai, Z. Yuan, N. Jiang, T. Li, Y. Wang, Y. Guo, Z. Li, S. Ma, D. Zhong, Y. Li and J. Wang, *J. Am. Chem. Soc.*, 2018, **140**(12), 4222–4226; (c) P. J. Evans, J. Ouyang, L. Favereau, J. Crassous, I. Fernández, J. P. Hernáez and N. Martin, *Angew. Chem., Int. Ed.*, 2018, **57**, 6774–6779.
3 (a) K. Kawasumi, Q. Zhang, Y. Segawa, L. T. Scott and K. Itami, *Nat. Chem.*, 2013, **5**, 739–744; (b) M. A. Medel, R. Tapia, V. Blanco, D. Miguel, S. P. Morcillo and A. G. Campaña, *Angew. Chem., Int. Ed.*, 2021, **60**, 6094–6100; (c) Z. Qiu, S. Asako, Y. Hu, C. W. Ju, T. Liu, L. Rondin, D. Schollmeyer, J. S. Lauret, K. Müllen and A. J. Narita, *J. Am. Chem. Soc.*, 2020, **142**(35), 14814–14819; (d) N. Ogawa, Y. Yamaoka, H. Takikawa, K. Yamada and K. Takasu, *J. Am. Chem. Soc.*, 2020, **142**(31), 13322–13327; (e) J. Ma, Y. Fu, E. Dmitrieva, F. Liu, H. Komber, F. Hennersdorf, A. A. Popov, J. J. Weigand, J. Liu and X. Feng, *Angew. Chem., Int. Ed.*, 2020, **59**, 5637–5642.
4 (a) W. Shi, F. Salerno, M. D. Ward, A. Santana-Bonilla, J. Wade, X. Hou, T. Liu, T. J. S. Dennis, A. J. Campbell, K. E. Jelfs and M. J. Fuchter, *Adv. Mater.*, 2021, **33**, 2004115; (b) V. Kiran, S. P. Mathew, S. R. Cohen, I. H. Delgado, J. Lacour and R. Naaman, *Adv. Mater.*, 2016, **28**, 1957–1962; (c) I. S. Sánchez, M. Šámal, J. Nejedlý, M. Karras, J. Klívar, J. Rybáček, M. Buděšínský, L. Bednárová, B. Seidlerová, I. G. Stará and I. Starý Oxahelicene, *Chem. Commun.*, 2017, **53**, 4370–4373.
5 M. Stępień, E. Gońka, M. Żyła and N. Sprutta, *Chem. Rev.*, 2016, **117**, 3479–3716.
6 (a) X. He, J. Borau-Garcia, A. Y. Y. Woo, S. Trudel and T. Baumgartner, *J. Am. Chem. Soc.*, 2013, **135**, 1137–1147; (b) T. Delouche, R. Mokrai, T. Roisnel, D. Tondelier, B. Geffroy, L. Nyulászi, Z. Benkő, M. Hissler and P.-A. Bouit, *J. – Eur. J.*, 2020, **26**, 1856–1863.
7 For 7-membered P-rings used as chiral ligands, see: (a) S. Gladiali, A. Dore, D. Fabbri, O. D. Lucchi and M. Massanero, *Tetrahedron: asymmetry*, 1994, **5**, 511–514; (b) P. Nareddy, L. Mantilli, L. Guénée and C. Mazet, *Angew. Chem., Int. Ed.*, 2012, **51**, 3826–3831.
8 K. Mereiter and M. Widhalm, *Bull. Chem. Soc. Jpn.*, 2003, **76**, 1233–1244.
9 Racemic phosphepine **1** appeared also in Novaled patents, see: M. Zöllner, *Eur. Pat. Appl.*, **2887412**, 2015.
10 For other phospha-helicenes see: (a) K. Nakano, H. Oyama, Y. Nishimura, S. Nakasako and K. Nozaki, *Angew. Chem., Int. Ed.*, 2012, **51**, 695–699; (b) Y. Sawada, S. Furumi, A. Takai, M. Takeuchi, K. Noguchi and K. Tanaka, *J. Am. Chem. Soc.*, 2012, **134**, 4080–4083; (c) K. Yavari, S. Moussa, B. Ben Hassine, P. Retailleau, A. Voituriez and A. Marinetti, *Angew. Chem., Int. Ed.*, 2012, **51**, 6748–6752.
11 Nomenclature is based on assignation of the configuration of the P-center (R_P/S_P) and the helicenoid backbone (M/P).
12 For axial to central chirality transfer involving stereogenic P-center, see: (a) T. Murai, T. Hayashi, K. Yamada, Y. Maekawa and M. Minoura, *Chem. Commun.*, 2014, **50**, 12473–12475 For other heteroatoms, see: (b) G. Delogu, O. D. Lucchi and G. Licini, *J. Chem. Soc., Chem. Commun.*, 1989, 411–412; (c) L. Pisani and S. Superchi, *Tetrahedron: Asymmetry*, 2008, **19**, 1784–1789.
13 (a) C. Goedicke and H. Stegemeyer, *Tetrahedron Lett.*, 1970, **11**, 937–940; (b) R. H. Martin and M.-J. Marchant, *Tetrahedron Lett.*, 1972, **13**, 3707–3708.
14 P. Ravat, R. Hinkelmann, D. Steinebrunner, A. Prescimone, I. Bodoky and M. Juríček, *Org. Lett.*, 2017, **19**(14), 3707–3710.
15 H. Kubo, T. Hirose and K. Matsuda, *Org. Lett.*, 2017, **19**(7), 1776–1779.
16 (a) K. Dhbaibi, L. Favereau and J. Crassous, *Chem. Rev.*, 2019, **119**, 8846–8953; (b) L. Arrico, L. Di Bari and F. Zinna, *Chem. – Eur. J.*, 2021, **27**, 2920–2934.
17 (a) K. Yavari, W. Delaunay, N. De Rycke, T. Reynaldo, P. Aillard, M. Srebro-Hooper, V. Y. Chang, G. Muller, D. Tondelier, B. Geffroy, A. Voituriez, A. Marinetti, M. Hissler and J. Crassous, *Chem. – Eur. J.*, 2019, **25**, 5303–5310; (b) S. Nishigaki, K. Murayama, Y. Shibata and K. Tanaka, *Mater. Chem. Front.*, 2018, **2**, 585–590.